Supplementary material

Tunnel magnetoresistive sensors with non-hysteretic resistance-magnetic field curves using noncollinear interlayer exchange coupling through RuFe spacers

Prabhanjan D. Kulkarni, and Tomoya Nakatani†

Research Center for Magnetic and Spintronic Materials, National Institute for Materials Science, 1-2-1 Senen, Tsukuba, Ibaraki 305-0047, Japan

†Corresponding author: nakatani.tomoya@nims.go.jp

---

1. Calculation of *R-H* curve

The *R-H* curves of the spin-valve structure shown in Fig. S1(a) were calculated by minimizing the total magnetic energy in the single magnetic domain regime, the Stoner-Wohlfarth model. Figure 1(b) shows the magnetization configuration under an external magnetic field, H, in the $+x$ direction. $\mathbf{m}_{xx}$ denotes the magnetization of each ferromagnetic (FM) layer. $\mathbf{m}_{PL1}$ and $\mathbf{m}_{PL3}$ are pinned in the $+x$ direction, and $\mathbf{m}_{RL}$ is pinned in the $-x$ direction through the antiparallel IEC through the Ru spacer between RL and PL3. $\mathbf{m}_{PL2}$ is pinned in either $\pm\theta_{ud}$ titled direction from $\mathbf{m}_{PL1}$ by the noncollinear IEC through the RuFe spacer. Then, FL receives a unidirectional magnetic anisotropy in the same direction as $\mathbf{m}_{PL2}$ by the orange-peel FM coupling through the AgSn spacer. In addition, the FL has a uniaxial anisotropy in the $\pm\theta_{ua}$ titled direction from $\mathbf{m}_{PL1}$ which is induced by the annealing under a magnetic field. An external magnetic field H is applied in the $\pm x$ direction.

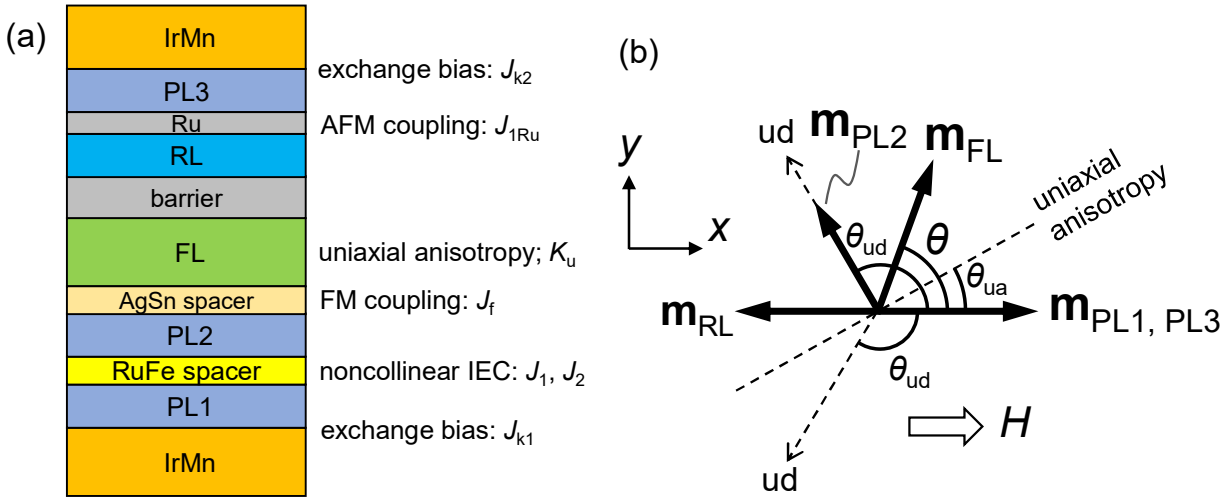

FIG. S1. (a) Layer structure and the energy terms. (b) Configuration of the magnetizations (**m**) of the ferromagnetic layers. θ_{ua} and θ_{ud} are the angles between the easy axes of the uniaxial and unidirectional anisotropies, respectively, and $\mathbf{m}_{PL1}$.

We define M as the saturation magnetization, t as the layer thickness, and θ as the angle between the magnetization and H for all the FM layers: PL1, PL2, FL, RL, PL3. We considered the following energy terms.

(1) Zeeman energy:

$$E_Z = -H(M_{\mathrm{PL1}}t_{\mathrm{PL1}}\cos\theta_{\mathrm{PL1}} + M_{\mathrm{PL2}}t_{\mathrm{PL}}\cos\theta_{\mathrm{PL2}} + M_{\mathrm{FL}}t_{\mathrm{FL}}\cos\theta_{\mathrm{FL}} + M_{\mathrm{RL}}t_{\mathrm{RL}}\cos\theta_{\mathrm{RL}} + M_{\mathrm{PL3}}t_{\mathrm{PL3}}\cos\theta_{\mathrm{PL3}}). \quad \text{(S1)}$$

(2) Exchange bias to PL1 and PL3:

$$E_{\mathrm{eb}} = -J_{\mathrm{k1}}\cos(\theta_{\mathrm{PL1}}) - J_{\mathrm{k3}}\cos(\theta_{\mathrm{PL3}}), \quad \text{(S2)}$$

where J_{k1} and J_{k3} represent the exchange bias energies at the IrMn/PL1 and PL3/IrMn interfaces.

(3) Noncollinear IEC between PL1 and PL2 through the RuFe spacer:

$$E_{\mathrm{ncIEC}} = -J_1\cos(\theta_{\mathrm{PL2}} - \theta_{\mathrm{PL1}}) - J_2\cos^2(\theta_{\mathrm{PL2}} - \theta_{\mathrm{PL1}}), \quad \text{(S3)}$$

where, J_1 and J_2 are the bilinear and biquadratic IEC energies, respectively.

(4) Orange-peel FM coupling between PL2 and FL through the AgSn spacer:

$$E_f = -J_{\mathrm{f}}\cos(\theta_{\mathrm{FL}} - \theta_{\mathrm{PL2}}), \quad \text{(S4)}$$

where J_f is the bilinear IEC energy.

(5) Uniaxial anisotropy of FL:

$$E_{\mathrm{ua}} = K_{\mathrm{u}} t_{FL} \sin^2(\theta_{\mathrm{FL}} - \theta_{\mathrm{ua}}), \quad \text{(S5)}$$

where, K_{u} is the anisotropy energy.

(6) Antiferromagnetic IEC between RL and PL3 through the Ru spacer:

$$E_{\mathrm{RuIEC}} = -J_{1\mathrm{Ru}} \cos(\theta_{\mathrm{RL}} - \theta_{\mathrm{PL3}}), \quad \text{(S6)}$$

where, $J_{1\mathrm{Ru}}$ is the bilinear IEC energy.

For simplicity, we assume that the magnetizations of PL1, RL, and PL3 are pinned in the original directions under the applied H; therefore, $\theta_{\mathrm{PL1}} = \theta_{\mathrm{PL2}} = 0$, and $\theta_{\mathrm{RL}} = \pi$. Then, the total magnetic energy equation is simplified to

$$E_{\mathrm{total}} = -H(M_{\mathrm{PL1}} t_{\mathrm{PL1}} - M_{\mathrm{RL}} t_{\mathrm{RL}} + M_{\mathrm{PL3}} t_{\mathrm{PL3}} + M_{\mathrm{PL2}} t_{\mathrm{PL2}} \cos\theta_{\mathrm{PL2}} + M_{\mathrm{FL}} t_{\mathrm{FL}} \cos\theta_{\mathrm{FL}}) + K_{\mathrm{u}} t_{\mathrm{FL}} \sin^2(\theta_{\mathrm{FL}} - \theta_{\mathrm{ua}}) - J_1 \cos\theta_{\mathrm{PL2}} - J_2 \cos^2\theta_{\mathrm{PL2}} - J_{\mathrm{f}} \cos(\theta_{\mathrm{FL}} - \theta_{\mathrm{PL2}}) \ . \quad \text{(S7)}$$

Based on the experimental data, we used the following values: $M_{\mathrm{FL}} t_{\mathrm{FL}}$ = 49.5 T nm, $M_{\mathrm{PL1}} t_{\mathrm{PL1}} = M_{\mathrm{PL2}} t_{\mathrm{PL2}} = M_{\mathrm{RL}} t_{\mathrm{RL}} = M_{\mathrm{PL3}} t_{\mathrm{PL3}} = 6$ T nm (1 T nm = 7.95×10^{-5} emu/cm^2), J_{f} = 0.1 mJ/m^2, and $K_{\mathrm{u}} t_{\mathrm{FL}}$ = 0.03 mJ/m^2, corresponding to an anisotropy field (H_k) of 1.5 mT from the relationship of $K_{\mathrm{u}} t_{\mathrm{FL}} = H_{\mathrm{k}} M_{\mathrm{FL}} t_{\mathrm{FL}}/2$. For the noncollinear IEC through the RuFe spacer, J_1 was varied, while J_2 was fixed to –0.35 mJ/m^2. This J_2 value is somewhat larger than the experimentally obtained values of about –0.3 mJ/m^2 for the $\mathrm{Ru}_{100-x}\mathrm{Fe}_x$ (x = 54–70 at. %) spacers in the CIP-GMR films (Fig. 1). The choice of J_2 = –0.35 mJ/m^2 for the simulations was because $\mathbf{m}_{\mathrm{RL}}$ is slightly rotated for –0.3 mJ/m^2, which complicates the interpretation of the results. Since the anisotropy field of the FL is determined only by J_{f}, the use of a larger value of J_2 than that by the experiment does not significantly affect the simulation results.

Recalling that θ_{ud} is the angle between the $\mathbf{m}_{\mathrm{PL1}}$ and $\mathbf{m}_{\mathrm{PL2}}$, and the $\mathbf{m}_{\mathrm{PL1}}$ is pinned in the +x direction, we obtain $\theta_{\mathrm{ud}} = (\theta_{\mathrm{PL2}} - \theta_{\mathrm{PL1}})_{H=0} = (\theta_{\mathrm{PL2}})_{H=0}$. In addition, θ_{ud} follows [1, 2]

$\theta_{\mathrm{ud}} = 0$ when $J_1/J_2 < -2$,

$\theta_{\mathrm{ud}} = \pi$ when $J_1/J_2 > 2$,

$$\theta_{\mathrm{ud}} = \cos^{-1}(-J_1/2J_2) \qquad \text{when } 2 \geq J_1/J_2 \geq -2. \qquad \text{(S8)}$$

Therefore, for the calculations of the *R*-*H* curve, θ_{ud} was varied from 0 to π by changing J_1/J_2 from –2 to 2.

By minimizing E_{total} in Eq. (S7), we obtained θ_{FL} at different H. The *R*-*H* curves were calculated by

$$R = 1/\left[\frac{G_{\max}+G_{\min}}{2} + \frac{G_{\max}-G_{\min}}{2}\cos(\theta_{\mathrm{RL}} - \theta_{\mathrm{FL}})\right], \qquad \text{(S9)}$$

where, $G_{\max}$ and $G_{\min}$ are the maximum and minimum values of the tunnel conductance in the parallel and antiparallel magnetization state between $\mathbf{m}_{\mathrm{FL}}$ and $\mathbf{m}_{\mathrm{RL}}$, respectively, and $\theta_{\mathrm{RL}} = \pi$. In this paper, we used $G_{\min} = 1$ and $G_{\max} = 2.8$ (i.e., TMR ratio = 180%). The calculated *R*-*H* curves for variations of θ_{ud} and θ_{ua} were numerically differentiated, and the sensitivity, $\frac{dR}{dH}\frac{1}{R}$, was calculated.

2. Supplementary data: Hysteresis of the TMR device shown in Fig. 4(b)

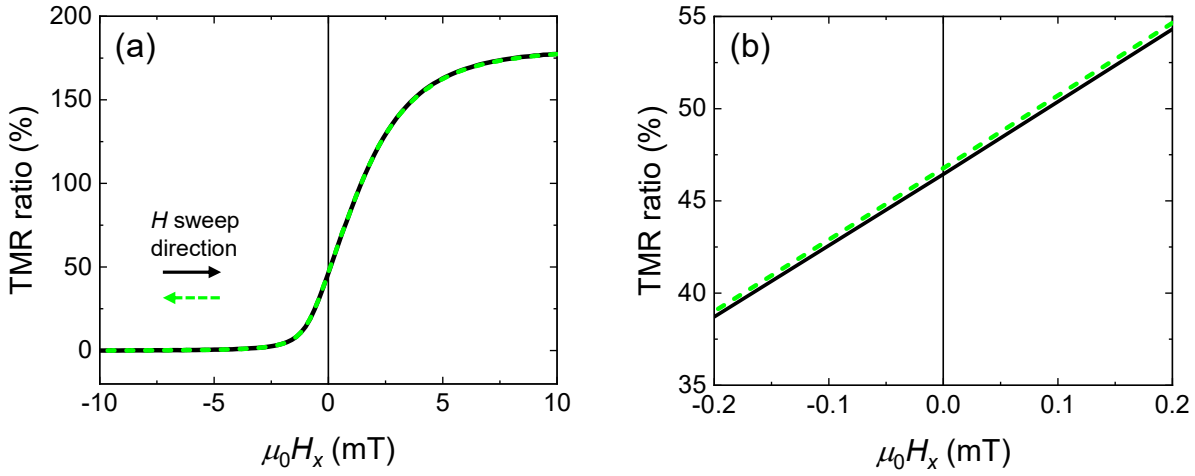

FIG. S2. (a) Full TMR curve of the device shown in Fig. 4(b) (θ_{ud} ~ ±120° and θ_{ua} = 60°), showing negligible magnetic hysteresis. (b) The same curve zoomed in small H_x range.

References

[1] E.E. Fullerton and S.D. Bader, Phys. Rev. B **53**, 5112 (1996).

[2] P.D. Kulkarni, T. Nakatani, T. Sasaki, and Y. Sakuraba, J. Appl. Phys. **129**, 213901 (2021).